Evaluation of Effects of TGF-β1 Inhibition on Gastric Cancer in Nude Mice by Diffusion Kurtosis Imaging and In-Line X-ray Phase Contrast Imaging With Sequential Histology

Bowen Shi, MD,[1] Fei Yuan, MD,[2] Fuhua Yan, MD,[1] Huan Zhang, MD,[1] Zilai Pan, MD,[1] Weibo Chen, PhD,[3] Guilong Wang, PhD,[3] Jingwen Tan, MD,[1] Yang Zhang, MD,[1] Yuqi Ren, PhD,[4]* and Lianjun Du, MD[1]*

Background: Accurate and complete response evaluation after treatment is important to implement individualized therapy for gastric cancer.
Purpose: To investigate the effectiveness of diffusion kurtosis imaging (DKI) and in-line X-ray phase contrast imaging (ILXPCI) in the assessment of the therapeutic efficacy by transforming growth factor beta 1 (TGF-β1) inhibition.
Study Type: Prospective animal study.
Animal Model: Thirty nude mice subcutaneous xenotransplantation tumor model of gastric cancer for DKI and 10 peritoneal metastasis nude mice model for ILXPCI.
Field Strength/Sequence: Examinations before and serially at 7, 14, 21, and 28 days after TGF-β1 inhibition treatment were performed at 3T MRI including T_2-weighted imaging (T_2WI) and DKI with five b values of 0, 500, 1000, 1500, 2000 s/mm^2; ILXPCI examinations were performed at 14 days after treatment.
Assessment: DKI parameters (apparent diffusion coefficient [ADC], diffusivity [D] and kurtosis [K]) were calculated by two experienced radiologists after postprocessing.
Statistical Tests: For the differences in all the parameters between the baseline and each timepoint for both the treated and the control mice, the Mann–Whitney test was used. The Spearman correlation test was used to evaluate correlations among the DKI parameters and corresponding pathologic necrosis fraction (NF).
Results: ADC, D, and K values were significantly different between the two groups after treatment ($P < 0.05$). Serial measurements in the treated group showed that the ADC, D, and K values were significantly different at 7, 14, 21, and 28 days compared with baseline ($P < 0.05$). There were significant correlations between DKI parameters and NF (ADC, $r = 0.865$, $P < 0.001$; D, $r = 0.802$, $P < 0.001$; K, $r = -0.944$, $P < 0.001$). The ILXPCI results in the treated group showed a stronger absorption area than the control group.
Data Conclusion: DKI may be used to evaluate the complete course therapeutic effects of gastric cancer induced by TGF-β1 inhibition, and the ILXPCI technique will improve the tumor microstructure resolution.
Level of Evidence: 1
Technical Efficacy: Stage 4

*Address reprint requests to: L.D., Department of Radiology, Ruijin Hospital, Shanghai Jiao Tong University School of Medicine Shanghai, Shanghai, 200025, P.R. China. E-mail: lianjundu@163.com; or Y.R., Shanghai Institute of Applied Physics, Chinese Academy of Sciences, Shanghai, 200025, P.R. China. e-mail: renyuqi@sinap.ac.cn
The first two authors contributed equally to this work.
The last two authors contributed equally to this work.

From the [1]Department of Radiology, Ruijin Hospital, Shanghai Jiao Tong University School of Medicine, Shanghai, P.R. China; [2]Department of Pathology, RuiJin Hospital, Shanghai Jiao Tong University School of Medicine, Shanghai, P.R. China; [3]Philips Healthcare, Shanghai, P.R. China; and [4]Shanghai Institute of Applied Physics, Chinese Academy of Sciences, Shanghai, P.R. China

Additional supporting information may be found in the online version of this article.

Despite many advances in cancer diagnosis and treatment, gastric cancer currently remains the fourth most common malignancy and the second leading cause of cancer-related death worldwide.[1,2] Previous research has established that transforming growth factor beta (TGF-β) signaling is a key player in epithelial-mesenchymal transition (EMT)-related chemotherapy and targeted therapy resistance in a number of malignancies.[3,4] TGF-β1 levels are correlated with peritoneal metastasis and with the TNM stages of gastric cancer.[5] Research also suggests that the expression of TGF-β1 influences EMT initiation and that it intervenes in the progress of gastric cancer metastasis.

Therefore, we hypothesized that inhibiting TGF-β1 signaling activation will influence the process of gastric tumor growth, and the therapeutic response was observed with multimodal imaging methods.[6] Multiple imaging methods, such as computed tomography (CT), magnetic resonance imaging (MRI), and positron emission tomography (PET) all play an indispensable role in the diagnosis of disease by virtue of their own characteristics and advantages. The response evaluation criteria in solid tumors (RECIST) is the widely adopted standard for evaluating therapy response based on the change in tumor size in clinical practice, but the evaluation period often takes several weeks to months to develop.[7] Therefore, increasing demands are being placed on imaging modalities to identify reliable surrogate markers for the evaluation of complete therapeutic effect in patients with gastric cancer. The accuracy of diagnosis and the therapeutic evaluation of imaging modalities is essential for individualized treatment planning in patients with gastric cancer. Although the intervention effect with a TGF-β1 inhibitor for tumors was proven effective in previous studies,[8] understanding how to use imaging technology to assess its therapeutic effect has not been reported.

Currently, tumor imaging techniques are used to predict the response of gastric cancer to treatment,[9] and functional imaging has been used to evaluate tissue morphological changes. Exploring various functional magnetic resonance imaging (fMRI) modalities made it possible to detect the microstructural changes before the morphological changes, which may be useful for clinicians to predict therapy response. Diffusion-weighted imaging (DWI) is capable of providing an apparent diffusion coefficient (ADC), which is verified to effectively detect the in vivo water motion restriction and has also become an optimal choice for monitoring the tumoral response to treatment.[10–12] The classical DWI model is based on the assumption that water diffusion follows a Gaussian distribution. Water diffusion, in vivo, is normally restricted by the tissue microstructures, such as cell membranes and cell density, such that the real diffusion is much more complex than the standard Gaussian distribution. DKI is a non-Gaussian diffusion-weighted model that was first proposed by Jensen et al.[13] This imaging analysis method is considered to account for the non-Gaussian diffusion property resulting from the microstructural complexity of tissue structures, and the model includes a calculation of the kurtosis and diffusivity coefficients. The kurtosis parameter reflects the deviation of the diffusion property from a normal distribution in restricted water diffusion, the value is related to the complexity of the internal organizational structure of ROI, and the diffusion limitation of non-Gaussian water molecules is more significant as the complexity of the structure in the ROI increases. The diffusivity is the diffusion coefficient with a correction of a non-Gaussian bias. DKI shows a substantially higher sensitivity than that shown with conventional DWI for cancer detection in evaluating gliomas,[14] prostate cancer,[15] and breast lesions.[16] To our knowledge, there have been a few studies on the use of DKI for assessing the early response of a tumor to treatment, and also suggests that kurtosis has a highly positive association with histologic grade.[17,18] However, most of the tumor therapy strategies have a long cycle of chemotherapy treatment. There are few studies on the long-term efficacy evaluation of gastric cancer and the functional imaging evaluation of cancer treatment.

However, the image resolution of the current examination methods is on the millimeter-scale, and these current imaging methods have profound limitations in detecting the tumor peritoneal metastatic and microstructure changes of tumor tissues. As a new imaging method, in-line X-ray phase-contrast imaging (ILXPCI) has a high spatial resolution and density resolution, which provides high contrast images by using the phase shift of the X-ray.[19] The image resolution that can be achieved by X-ray phase contrast microtomography is on the micron-scale. ILXPCI largely improves the image quality of soft tissues, particularly at the interface of the tissues, where the refractive index changes significantly.[20,21] Therefore, soft tissue imaging using ILXPCI has potential use in clinical applications. However, the treatment assessment of peritoneal tumors has not yet been studied.

Therefore, the purpose of our experiments was to explore the correlation between the imaging and the histologic results and to further test the effectiveness of the DKI parameters as potential imaging markers in the assessment of the complete therapeutic efficacy of a TGF-β1 inhibitor (SB431542) in a nude mouse gastric cancer model. We also evaluated the tumor morphological characteristics with treatment in a human gastric tumor peritoneal metastasis model using ILXPCI.

Materials and Methods

Cell Culture
The moderately differentiated MGC-803 human gastric cancer cell lines were cultured in RPMI 1640 medium, supplemented with 10% fetal bovine serum, 100 units/mL streptomycin, and 100 μg/mL penicillin at 37°C in a humidified atmosphere with 5% CO_2.

Gastric Cancer Xenograft Animal Model
All the experimental protocols were approved by the Institutional Animal Care and Use Committee. Thirty male (6-week-old) athymic

nude mice, weighing 20–25 g, were housed under a specific pathogen-free environment in the animal laboratory. All the mice were subcutaneously injected with 2×10^6 human gastric MGC-803 cells in 200 μL serum-free media into the right front side.

TGF-β1 Inhibitor Preparation and Treatment
The tumors were allowed to grow to 200 mm^3 before the treatment, and a total of 30 mice with gastric cancer xenograft tumors were randomly divided into the control group (n = 15) and the treatment group (n = 15). In this study the mice in the treated group were administered with TGF-β1 Inhibitor (SB431542) by a tail intravenous injection, at a dosage of 20 mg/kg once daily for the first week; then the injections were administered twice a week. The mice in the control group were administered with sterilized water at the same dosage.

MR Image Techniques
All the MRI examinations were performed with a 3.0T MRI system (Ingenia, Philips Healthcare, Best, The Netherlands) with a 16-channel human wrist coil. Follow-up MRI studies were performed before treatment (day 0, baseline) and at 7, 14, 21, and 28 days after treatment. All the experimental mice were anesthetized with an intraperitoneal injection of pentobarbital sodium (50 mg/kg body weight). The protocol included the axial fast-spin echo (FSE) T$_2$-weighted imaging (T$_2$WI) and the axial DKI examination. A transverse T$_2$-weighted image was obtained using the fast spin echo (FSE) sequence (repetition time / echo time [TR/TE], 3000/100 msec; field of view [FOV], 60 × 60 mm, section thickness, 2 mm; matrix size, 240 × 182; NSA, 5; intersection gap, 0.2 mm; and bandwidth = 257.8 Hz/pixel). Subsequently, the DKI sequences were obtained by using single-shot echo-planar imaging, with 5 b-values of 0, 500, 1000, 1500, and 2000 s/mm^2, as well as the number of signal averages that included one average (b value of 0–499 s/mm^2), two averages (b value of 500–999 s/mm^2), and three averages (b value of 1000–2000 s/mm^2) were performed.[22] The following parameters were used for this sequence: TR/TE = 2700/100 msec; FOV = 60 × 60 mm; section thickness = 2 mm; matrix size = 88 × 75; NSA = 5; intersection gap = 0.2 mm; bandwidth = 17.8 Hz/pixel; parallel imaging SENSE factor = 2.5 and number of slices = 10. The total time for the DKI scanning for each study was 7 minutes.

DKI Parametric Map Acquisition
All the DKI parameters, including the apparent diffusion coefficient (ADC), diffusivity (D), and kurtosis (K) were postprocessed using a manufacturer-supplied software (PRIDE DWI Tool, v. 1.5, Philips Healthcare).[23] For the DKI dataset, a three-variable linear least-square method was performed, including voxel-by-voxel analysis, the fitting diffusion-weighted signal intensities as a function of the b-value used to calculate pixel-wise kurtosis, and the diffusivity maps based on the DKI model, which was applied in a previous study[13] using the following equation: $S = S_0 \times \exp(- b \times D + b^2 \times D^2 \times K/6)$, where S is the DWI signal at a particular b value, S$_0$ is the baseline signal without the diffusion weighting, D is the diffusivity, and K is the kurtosis. In this model, D represents the corrected ADC accounting for the non-Gaussian diffusion behavior and is a corrected ADC that removes this non-Gaussian bias. The kurtosis

parameter is a unitless parameter that quantifies the deviation of the water motion from the Gaussian diffusion, and a larger K represents a greater deviation from the Gaussian distribution. This program also calculated the ADC for each pixel using the standard monoexponential fit with the equation: $S = S_0 * \exp(-b * ADC)$.

Quantitative Measurement and Image Analysis
For the quantitative image analysis, the final results of all the parameters, including the ADC, D, and K, were measured by two radiologists, who were blinded to the information regarding the treated and control groups. The drawing was done three times at the same slice and the measured values were averaged by each reader. After a 2-week interval, these measurements were repeated and the final averaged values were calculated by each reader. The conventional T$_2$-weighted MR images and the DKI diffusion maps (b = 1000 s/mm^2) were used as references to determine the lesion areas on the corresponding DKI parametric maps. The most restricted diffusion area (MRDA) was drawn on the DKI maps as the region of interest (ROI)[24,25] of the tumor in both groups at 14 days (Figs. 1–2) and 28 days (Supplementary Figs. 1, 2). The ROIs were copied from the DKI diffusion maps and were placed on the other corresponding parametric maps of the ADC, D, and K. When applying the ROI method, the parameter values multiplied by the corresponding ROI voxel was derived and defined as the single-slice ROI result. ROIs were delineated on five consecutive slices selected from the center of the tumor where the tumor images are clear. The final each parameter value was determined as the mean value in the delineated ROI results by integrating all tumor voxels from all delineated slices into the total signal intensity.[22,26] To evaluate the therapeutic response based on RECIST guidelines, tumor size defined by the longest dimension on axial T$_2$W images was measured and recorded.[27,28] A set of source DKI diffusion images and the ROI-based fitted curves was drawn by using the manufacturer-supplied software (PRIDE DWI Tool, v. 1.5, Philips Healthcare) (Supplementary Figs. 3, 4).

X-ray In-Line Phase Contrast Imaging Setting
A total of 10 nude mice were randomly divided into two groups for our experiments. The peritoneal metastasis xenograft model group was established by administering 150 μL (2×10^6 cells/mL) of a suspension of MGC-803 cells via the abdominal cavity. The mice in the treated group were administered the TGF-β1 inhibitor SB431542 after a period of 2 weeks of growth by an intraperitoneal injection at a dosage of 100 μL/10 g per body weight every other day, while the mice in the control group were administered sterilized water at the same dosage. Each group was sacrificed at 14 days after treatment. The tumor specimens were immersed in 4% formaldehyde for tissue fixation at room temperature overnight. The next day, the samples were washed and dehydrated using graded ethanol for ILXPCI.

The synchrotron radiation facility imaging device (Shanghai Synchrotron Radiation Facility) was a third-generation synchrotron source that mainly produced 2D images of the biological tissues using ILXPCI. The energy of the coherent monochromatic light generated by the double crystal monochromator was set to 15 keV. The detector, with an effective pixel size of 6.5 μm, was placed 20 cm downstream from the specimen. The exposure time of 2 seconds was adopted. All the projection images were transformed into
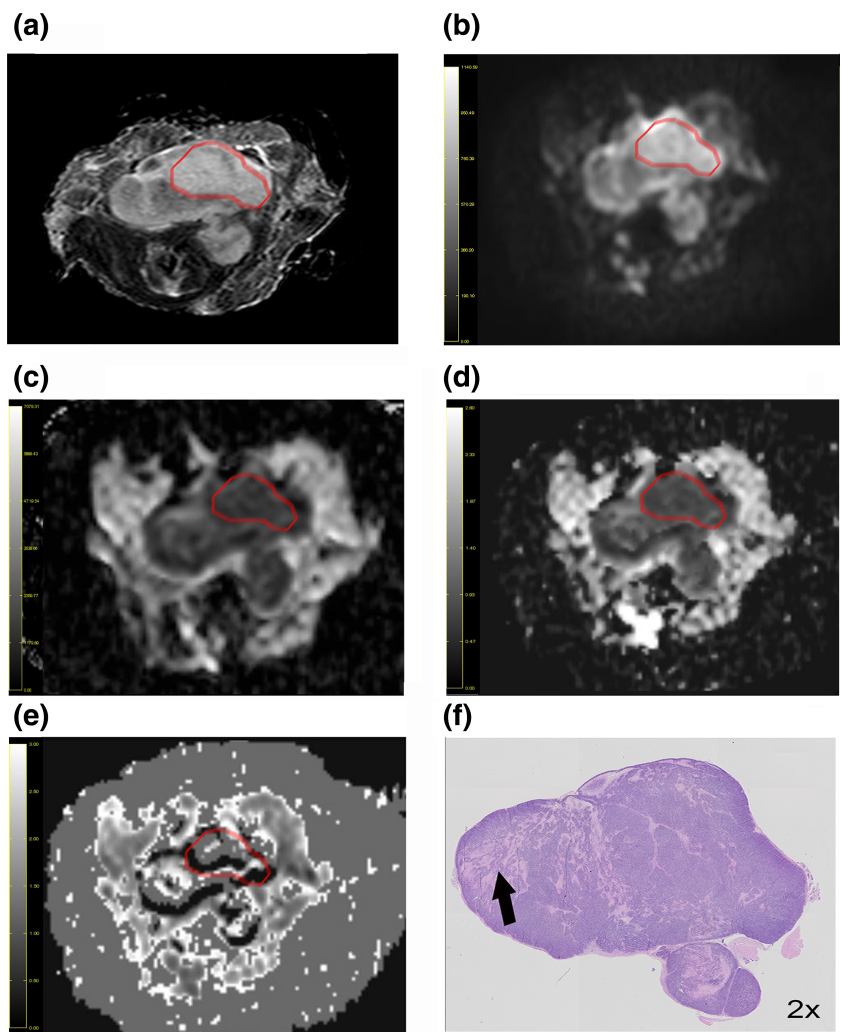
FIGURE 1: T$_2$-weighted imaging (T$_2$WI) axial image and diffusion kurtosis imaging (DKI) images with region of interest (ROI), and pathologic image of nude mouse in the treated group at 14 days. **a:** T$_2$WI axial image shows the tumor ROI (red circle). **b:** DKI diffusion map (b = 1000 s/mm^2). **c:** Apparent diffusion coefficient (ADC) map (ADC = 1.164 ± 0.051 × 10^{-3} mm^2/s). **d:** Diffusivity (D) map (D = 1.194 ± 0.036 × 10^{-3} mm^2/s). **e:** Kurtosis (K) map (K = 1.089 ± 0.093). **f:** Hematoxylin and eosin staining shows the necrotic area (black arrow) in the tumor (magnification 2×).

digital slice sections using the fast slice reconstruction software PITRE, based on the filtered back projection (FBP) algorithm. A 3D reconstruction was obtained using the 3D reconstruction software Amira (v. 5.3.3, ThermoFisher Scientific, Waltham, MA).

Histologic Evaluation

The experimental mice were euthanized by means of an intraperitoneal injection with pentobarbital sodium for histological examination. After fixation in 4% paraformaldehyde solution for at least 24 hours, the subcutaneous tumors were sliced with a slice thickness of 4 μm along the same orientation of the axial T$_2$WI imaging and was stained with hematoxylin and eosin (H&E) according to the standardized procedures. The H&E staining analysis was digitized with an optical magnification image acquisition system and was performed at 2× magnification to evaluate the NF of the tumor. The NF of the tumor was defined as the percent area of necrosis relative to the total area of the tumor sections with ImageJ software (http://imagej.nih.gov/ij). Tumor pathologic NF was scored according to the following formula: NF = Area$_{necrosis}$/Area$_{total\ tumor}$.[28] To ensure

the proper correlation between the pathologic and MRI features, these specimens were reviewed by the consultant pathologists.

Statistical Analysis

To evaluate the reproducibility of the DKI parameters of the tumors, the intra- and interobserver agreement in ROI measurements was calculated to derive the data variability for the two observers. The observers selected all the mice to evaluate the parameters with a two-way mixed consistency model in the treated group. An interclass correlation coefficient greater than 0.75 indicated good agreement.[29]

The differences in tumor size, NF at each timepoint between the treated group and the control groups, were evaluated with a Mann–Whitney test. For the differences in all the parameters between the baseline and each timepoint for both the treated and the control mice, the Kruskal–Wallis test or Mann–Whitney test was used. Spearman's correlation coefficient test was used to determine the correlations among NF and the corresponding DKI parameters of all the tumors from baseline to the end of follow-up. The correlation coefficient rho (r) was obtained to define the degree of
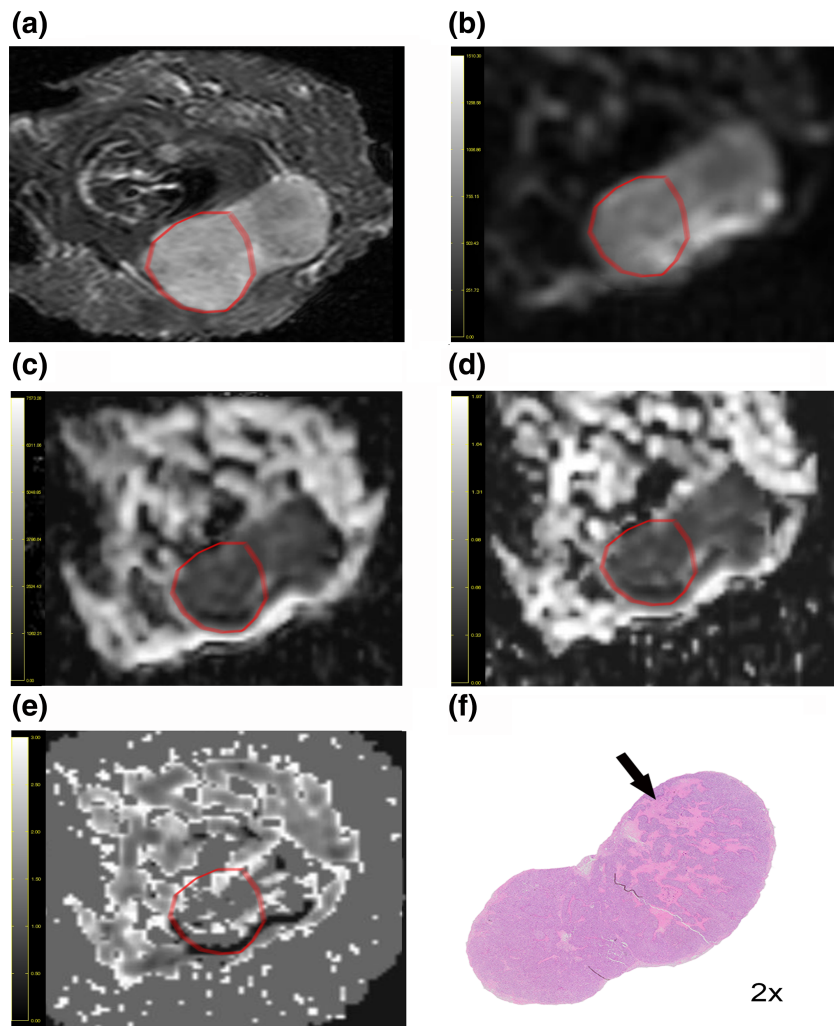
FIGURE 2: T_2WI axial image and DKI images with ROI, and pathologic image of nude mouse in the control group at 14 days. a: T_2WI axial image shows the tumor ROI (red circle). b: DKI diffusion map (b = 1000 s/mm^2). c: ADC map (ADC = 0.897 ± 0.058 × 10^{-3} mm^2/s). d: D map (D = 0.893 ± 0.083 × 10^{-3} mm^2/s). e: K map (K = 1.616 ± 0.071). f: Hematoxylin and eosin staining shows the necrotic area (black arrow) in the tumor (magnification 2×).

correlation as follows: 0.199 or less represented a poor or no relationship; 0.200–0.399 was weak; 0.400–0.599 was moderate; 0.600–0.799 was strong; and 0.8 or higher was excellent.[30]

The statistical analysis was performed using statistics software (SPSS v. 18.0; IBM, Armonk, NY). $P < 0.05$ indicated statistical significance.

Results

High intra- and interobserver intraclass correlation coefficient (ICC) for measuring all parameters in the treated group and baseline were observed. ICCs were found in all the mice in the treated group that underwent repeat MR measurements; the intraobserver agreement on ADC, D, and K values showed good reproducibility for reader 1 (ADC, 0.926, $P < 0.001$; D, 0.942, $P < 0.001$, and K, 0.963, $P < 0.001$), and reader 2 (ADC, 0.935, $P < 0.001$; D, 0.957, $P < 0.001$, and K, 0.977, $P < 0.001$). ICCs were found in all the mice in the treated group that underwent repeat MR measurements; the ADC, D, and K values showed good

reproducibility, with ICC values between the two observers of 0.902, $P < 0.001$; 0.941, $P < 0.001$, and 0.986, $P < 0.001$.

Effects of TGF-β1 Inhibition on Tumor Size and Pathologic NF

As shown in Fig. 3a, the tumor size at baseline was 1.046 ± 0.180 cm. A significant decrease in the time-dependent increase in tumor growth rate was found in the treated group compared with the control group, and the tumor size in the treated group was significantly smaller than that in the control group at the same timepoint (7 days, 1.272 ± 0.847 cm vs. 1.576 ± 0.134 cm $P = 0.008$; 14 days, 1.465 ± 0.081 cm vs. 1.905 ± 0.126 cm, $P = 0.008$; 21 days, 1.618 ± 0.062 cm vs. 2.188 ± 0.237 cm, $P = 0.008$, 28 days, 1.828 ± 0.065 cm vs. 2.340 ± 0.172 cm, $P = 0.008$).

The pathologic NF in the treated and control groups is shown in Fig. 3b, and the NF at baseline was 11.8 ± 2.014%. A significantly larger NF was observed in the
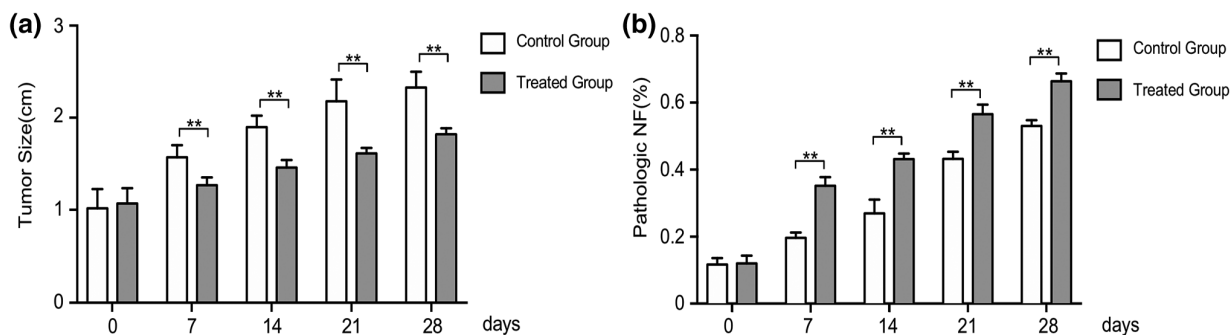
FIGURE 3: Bar graphs depicting the therapy effect throughout the TGF-β1 inhibition treatment. a: Tumor size changes, b: Pathologic necrosis fraction (NF). Comparisons between the two groups were performed using the Mann-Whitney test (*$P < 0.05$; **$P < 0.01$). Error bars denote standard errors of the mean.

treated group compared with the control group at the same timepoint (7 days, $35.2 \pm 2.304\%$ vs. $19.6 \pm 1.933\%$, $P = 0.008$; 14 days, $43.2 \pm 1.712\%$ vs. $27.0 \pm 4.080\%$, $P = 0.008$; 21 days, $56.7 \pm 2.857\%$ vs. $43.3 \pm 2.113\%$, $P = 0.008$, 28 days, $66.6 \pm 2.300\%$ vs. $53.2 \pm 1.756\%$, $P = 0.008$).

The tumor size in the treated group increased more slowly compared with the control group over time. No abnormality was found in the tumor specimen from H&E staining at baseline in both groups. In the last stage of treatment, the degree of necrosis in the treated group was significantly aggravated compared with that of the control group. H&E staining showed obvious massive coagulation necrosis after TGF-β1 inhibitor treatment. NF showed the same trend, revealing that the tumor necrosis degree in the treated group was more obvious than that in the control group.

Histological Assessment of the Tumor Response and Correlation With the DKI Parameters

The changes induced by the TGF-β1 inhibition treatment, as observed by DKI imaging, were compared with the corresponding histology. In the treated group, the ADC, D, and K values showed a significant correlation with the pathologic NF (Fig. 4). A significant relationship was observed between the K and NF ($r = -0.944$, $P < 0.001$), as well as between the ADC and D values, demonstrating a moderate relationship with NF (ADC, $r = 0.865$, $P < 0.001$; D, $r = 0.802$, $P < 0.001$). In the control group, there was no relationship among ADC, D, and K with NF (ADC, $r = 0.147$, $P = 0.483$; D, $r = 0.033$, $P = 0.874$ and K, $r = -0.382$, $P = 0.059$).

Comparison of the DKI Parameters Between the Treated and Control Groups

The values of the DKI parameters for both the treated and control groups at the same timepoint are summarized in Table 1. Compared with the control group, the K values significantly decreased in the treated group at 7 days ($P = 0.016$) and then showed a sustained decreased at the 14 days ($P = 0.009$), 21 days ($P = 0.009$), and 28 days
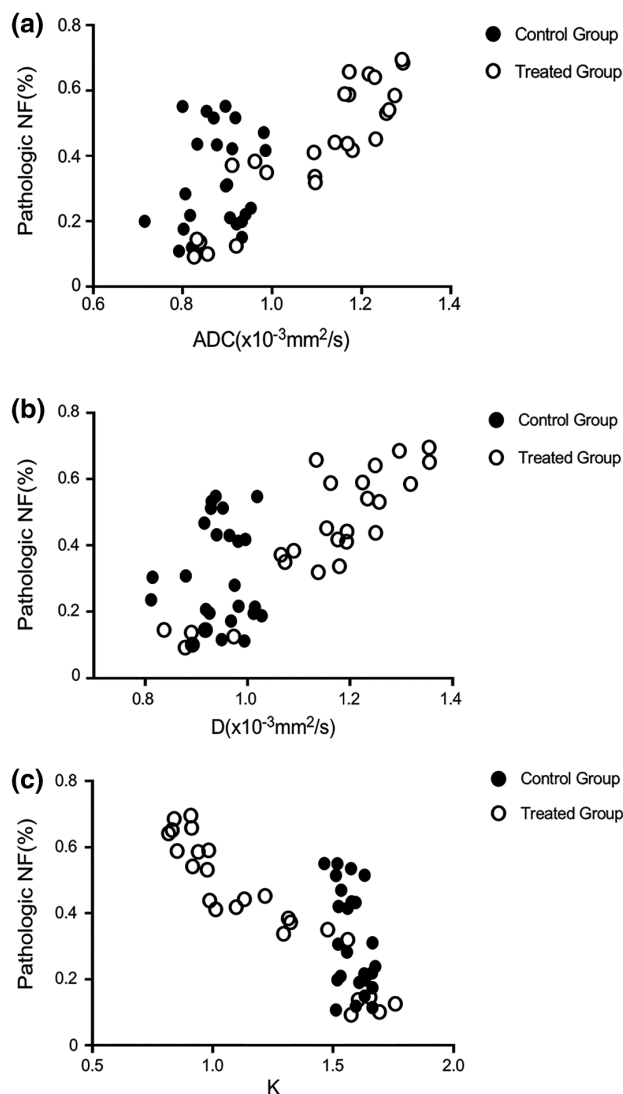

FIGURE 4: Correlation between DKI parameters and pathologic necrosis fraction (NF) in the treated and control groups. In the treated group, significantly correlations between ADC (a,d), D (b,e), K (c,f), and pathologic NF (ADC, $r = 0.865$, $P < 0.001$; D, $r = 0.802$, $P < 0.001$ and K, $r = -0.944$, $P < 0.001$) are found. In the control group, no correlations were found between ADC (a,d), D (b,e), K (c,f), and pathologic NF (ADC, $r = 0.147$, $P = 0.483$; D, $r = 0.033$, $P = 0.874$, and K, $r = -0.382$, $P = 0.059$).

TABLE 1. Comparison of DKI Imaging Parameters Between the Treated and Control Groups

Parameters	Treated group	Control group	P value
ADC($\times10^{-3}$mm^2/s)			
0 day	0.856 ± 0.038	0.817 ± 0.079	0.175
7 days	1.012 ± 0.083	0.874 ± 0.062	0.028
14 days	1.164 ± 0.051	0.897 ± 0.058	0.009
21 days	1.227 ± 0.064	0.916 ± 0.066	0.009
28 days	1.242 ± 0.051	0.866 ± 0.045	0.009
D($\times10^{-3}$mm^2/s)			
0 day	0.895 ± 0.050	0.936 ± 0.038	0.117
7 days	1.110 ± 0.048	0.988 ± 0.045	0.009
14 days	1.194 ± 0.036	0.893 ± 0.083	0.009
21 days	1.240 ± 0.056	0.960 ± 0.032	0.009
28 days	1.279 ± 0.092	0.954 ± 0.038	0.009
K			
0 day	1.656 ± 0.072	1.584 ± 0.068	0.175
7 days	1.394 ± 0.118	1.613 ± 0.050	0.016
14 days	1.089 ± 0.093	1.616 ± 0.071	0.009
21 days	0.934 ± 0.053	1.558 ± 0.029	0.009
28 days	0.862 ± 0.045	1.540 ± 0.064	0.009

Data expressed as mean ± standard deviation. Comparisons between control and treated groups at each time were performed by using the Mann-Whitney test. ADC: apparent diffusion coefficient; D: diffusivity; K: kurtosis.

follow-ups ($P = 0.009$). The ADC and D values were significantly higher in the treated group than in the control group at 7 days ($P = 0.028$, $P = 0.009$), 14 days ($P = 0.009$, $P = 0.009$), 21 days ($P = 0.009$, $P = 0.009$), and 28 days follow-ups ($P = 0.009$, $P = 0.009$).

To further explore the efficacy of the DKI parameters for monitoring the complete therapeutic effects of the TGF-β1 inhibitor on the tumors, sequential measurements of the DKI parameters of both the treated and control groups were carried out and the results were analyzed by a Mann–Whitney U-test. As shown in Table 2 and Fig. 5, the ADC and D values in the treated group gradually increased at 7 days, 14 days, 21 days, and 28 days compared with baseline after treatment (ADC, $P = 0.016$, 0.009, 0.009, and 0.009; D, $P = 0.009$, 0.009, 0.009, and 0.009, respectively). A significant increase in these two parameters was found at 14 days, 21 days, and 28 days vs. 7 days (ADC, $P = 0.028$, 0.009, and 0.009; D, $P = 0.028$, 0.016, and 0.028, respectively). However, no differences were found for both the ADC and D values between 21 days vs. 14 days ($P = 0.117$, 0.175), 28 days vs. 14 days ($P = 0.076$, 0.175), and 28 days vs. 21 days ($P = 0.465$, 0.347). The sequential K measurements significantly decreased at 7 days ($P = 0.009$) and slightly decreased at 14 days ($P = 0.009$), 21 days ($P = 0.009$), and 28 days ($P = 0.009$) compared with the values at baseline. The sequential K measurements were significantly lower at 14, 21, and 28 days ($P = 0.009$, 0.009, and 0.009, respectively) than that at 7 days. K also showed an obvious difference at 21 days vs. 14 days ($P = 0.009$), as well as 28 days vs. 14 days ($P = 0.009$) and 28 days vs. 21 days ($P = 0.028$). In the control group, serial changes in the DKI parameters showed no difference among all the timepoints.

Effect of TGF-β1 Inhibition on Peritoneal Metastasis by the ILXPCI

The resulting images from the peritoneal metastasis specimens using the ILXPCI in the treated and control groups are shown in Figs. 6 and 7. The tumor changes were distinctly observed at 14 days after TGF-β1 inhibitor treatment. The ILXPCI projection images of the two groups are presented in

TABLE 2. Sequential Measurements of DKI Parameters From Baseline, the Treated Group, and the Control Group and P Values for Comparisons Between Different Timepoints

Parameter	Treated group Measurement	P value 7 days	14 days	21 days	28 days	Control group Measurement	P value 7 days	14 days	21 days	28 days
ADC($\times 10^{-3}$mm^2/s)										
0 day	0.856 ± 0.038	0.016	0.009	0.009	0.009	0.817 ± 0.079	0.402	0.117	0.059	0.251
7 days	1.012 ± 0.083		0.028	0.009	0.009	0.874 ± 0.062		0.602	0.347	0.465
14 days	1.164 ± 0.051			0.117	0.076	0.897 ± 0.058			0.602	0.175
21 days	1.227 ± 0.064				0.465	0.916 ± 0.066				0.251
28 days	1.242 ± 0.051					0.866 ± 0.045				
D($\times 10^{-3}$mm^2/s)										
0 day	0.895 ± 0.050	0.009	0.009	0.009	0.009	0.936 ± 0.038	0.094	0.347	0.347	0.251
7 days	1.110 ± 0.048		0.028	0.016	0.028	0.988 ± 0.045		0.076	0.175	0.347
14 days	1.194 ± 0.036			0.175	0.175	0.893 ± 0.083			0.251	0.347
21 days	1.240 ± 0.056				0.347	0.960 ± 0.032				0.602
28 days	1.279 ± 0.092					0.954 ± 0.038				
K										
0 day	1.656 ± 0.072	0.009	0.009	0.009	0.009	1.584 ± 0.068	0.402	0.205	0.602	0.292
7 days	1.394 ± 0.118		0.009	0.009	0.009	1.613 ± 0.050		0.675	0.076	0.076
14 days	1.089 ± 0.093			0.009	0.009	1.616 ± 0.071			0.347	0.076
21 days	0.934 ± 0.053				0.028	1.558 ± 0.029				0.347
28 day	0.862 ± 0.045					1.540 ± 0.064				

Data were tested with Kruskal-Wallis test followed by Mann-Whitney U-test in the case of statistical significance. ADC: apparent diffusion coefficient; D: diffusivity; K: kurtosis.

Figs. 6a and 7a. Two typical slices, corresponding to the two groups, are shown in Figs. 6b and 7b. Figures 6c and 7c present a 3D structural reconstruction of the tumors at the different growth stages for the treated and control groups. The marked regions of Figs. 6b and 7b are the strong absorption areas, which are identified as calcium deposition, according to the H&E pathological staining images. The area of the tumor internal calcification and necrosis in the treated group was significantly larger than that in the control group.

Discussion

In conclusion, the aim of the present research was to examine the feasibility of DKI for the evaluation of the full therapeutic course of TGF-β1 inhibition therapy on gastric tumors in nude mice. Our results confirmed that DKI imaging might be able to simultaneously reflect the pathological changes in
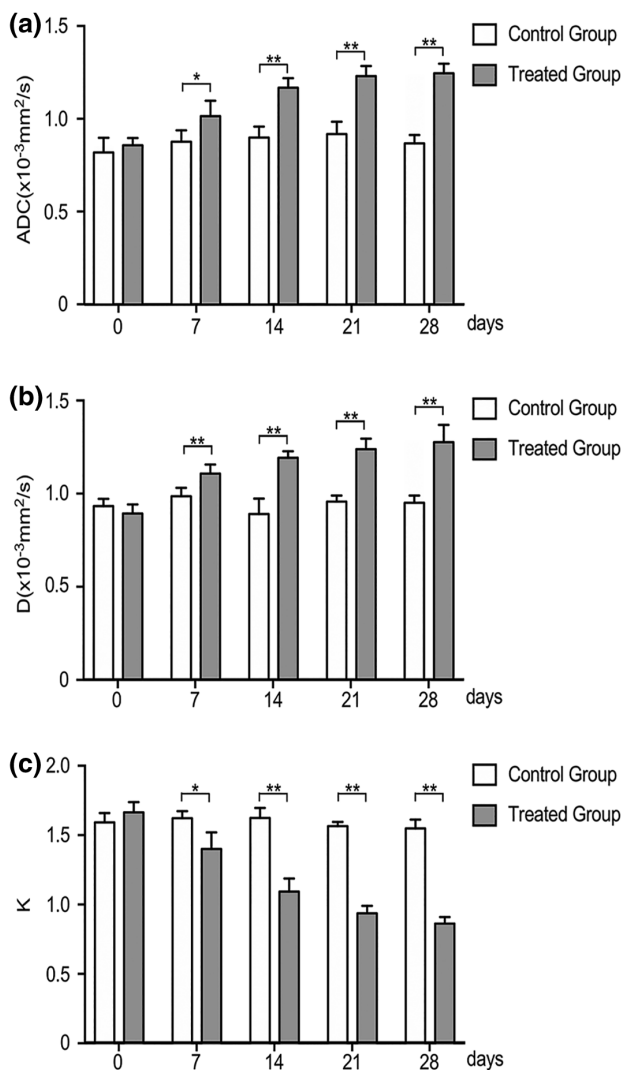

FIGURE 5: Bar graphs comparing changes in DKI parameters of the tumor, including (a) ADC, (b) D, and (c) K between the treated and control groups at each timepoint. Comparisons between the two groups were performed using the Mann-Whitney test (*$P < 0.05$; **$P < 0.01$). Error bars denote standard errors of the mean.

gastric cancer, resulting from the effects of the TGF-β1 inhibition, with a moderate to good reproducibility. The assessment of the change trend in the therapeutic efficacy with the DKI parameter was consistent with the pathological findings. The research also showed that the K value might be a potential parameter to differentiate the complete treatment response to gastric cancer xenografts, which suggests that DKI might have a larger utility than monoexponential DWI for predicting the treatment response of tumors. The ILXPCI is a new imaging method that shows the microstructure changes in biological tissues and has applications in the evaluation of the therapeutic effect on peritoneal metastasis.

The development of TGF-β1 targeted molecular inhibitors has become the focus of tumor mechanism research,[31] and the inhibition of the TGF-β1 signaling pathway promotes cell apoptosis and reduces the invasion and metastasis in gastric cancer.[32] Our pathological result confirmed that the tumor tissue had a more compact structure in the early stage, and the tissue necrosis degree after the TGF-β1 inhibition therapy was significantly stronger than that in the control group. Additionally, the distribution of the tumor cells was also less organized. In the late stage, the gross specimens of the treated group showed a looser structure, and a significant difference in tumor coagulative necrosis was observed between the two groups. The extent and degree of coagulative necrosis in the treated group increased significantly with the treatment cycle. The presence or absence of necrotic tissue in soft tissue tumors plays an important role in the determination of their biological characteristics and in the evaluation of therapeutic effects.[33]

Recent studies have shown that the ADC value derived from DWI signals may provide a quantitative method to achieve favorable treatment responses.[10–12] However, some studies found no significant difference between pretreatment ADC and tumor treatment response.[34,35] In addition, due to the microstructural complexity of tissue and cells, including cell membranes, intracellular organelles, and water compartments, the diffusion of water molecules tends to deviate from a Gaussian distribution. Conventional DWI assumes that water diffusion has a Gaussian distribution, thereby limiting the effectiveness of the technique in clinical use. Jensen et al[13] showed that diffusion kurtosis imaging provides a more complete characterization of the tissue profile in terms of cellularity and heterogeneity. It is believed that the DKI model obtained a better goodness of fit and showed more sensitivity to the tissue microstructural complexity for cancer detection.[36] In our study, we found that the ADC and D values of the tumor increased gradually in the treated group, while the K value decreased gradually. The tumor pathology results showed that the cell arrangement of the corresponding tumor parenchymal region was more loose and accompanied by necrosis in the treated group; as the cycle prolonged, the tumor necrosis area increased and the necrosis degree was
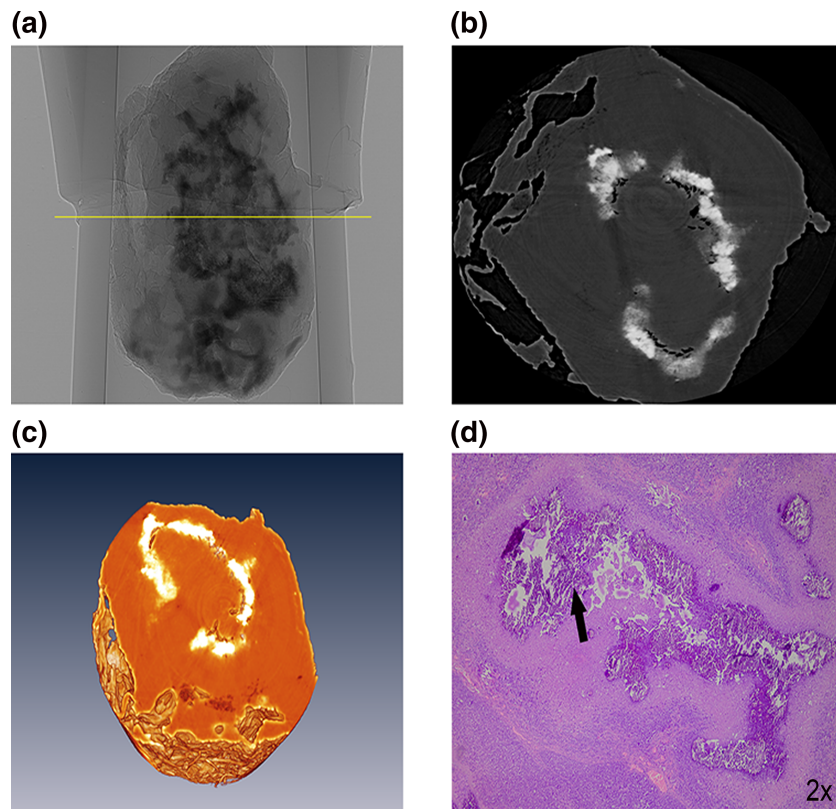
FIGURE 6: In-line X-ray phase contrast imaging (ILXPCI) and pathologic image of nude mouse peritoneal metastasis in the treated group at 14 days. a: An ILXPCI projective image of the specimen, horizontal line shows the slice we chose. b: The slice reconstruction image; white area shows the strong absorption. c: 3D-reconstruction image. d: Histopathological image; it shows the calcium deposition (black arrow).

more pronounced. This reflects that the degree of diffusion was more unrestricted than that of the early stage. The tendency of the DKI parameters change was consistent with the pathological results. These results further support the idea that DKI might be feasible for distinguishing microstructural-level damage to tumor tissue, and they might also reflect the whole process of TGF-β1 inhibition treatment in detail.

From the results, we saw that the ADC, D, and K were statistically significant in the comparison between the treatment group and the control group. On the one hand, the ADC and D values of the tumor after treatment were higher than the control group; we also found a significant increase in the ADC and D values during the course of the therapy as well as an excellent correlation with the NF. The relative changes in the ADC and D values are promising for the use of these values as predictors of the early treatment response to TGF-β1 inhibition. A similar effect is reported and confirmed by most studies on the utility of DWI in hepatic metastases and metastatic ovarian cancer.[37,38] However, the serial changes of the ADC and D values in the late period of treatment did not show any significant differences, and this result may be explained by the fact that the tumor morphology was affected by the effect of the drug therapy. The water diffusion capacity is limited due to tissue microstructure disorder. On the other hand, the K values of the tumor after treatment

were lower than the control group; the K parameter showed a significant decrease following the full treatment course, and there was a good positive correlation with the NF. The K parameter represents the deviation of the diffusion property from the Gaussian behavior and is believed to reflect the tissue microstructural complexity in more detail by a nonlinear fitting model.[17] The evaluation of the complete therapy of tumors has profound importance for clinical diagnosis and treatment, and we confirmed that the K not only evaluated the early curative effect but also had a certain importance for treatment in a long-term observation.

Currently, studies show that imaging evidence of the complete calcification of tumors may be a good indicator for chemotherapy responses.[39,40] Although MRI provides good contrast resolution and spatial resolution of soft tissues, MR image resolution only occurs at the millimeter scale. The spatial resolution of MRI to detect tissue calcification is very limited and is difficult to increase further. In this study, we saw the strong absorption change in local tissue imaging in the phased imaging for the treated group. The pathology confirmed the deposition of calcium deposits in the tumor tissue. The calcium deposition in the treated group was significantly higher than in the control group. From the results, we found that the ILXPCI provided high-contrast resolution and spatial resolution and that the subtle structure of the tumor tissues
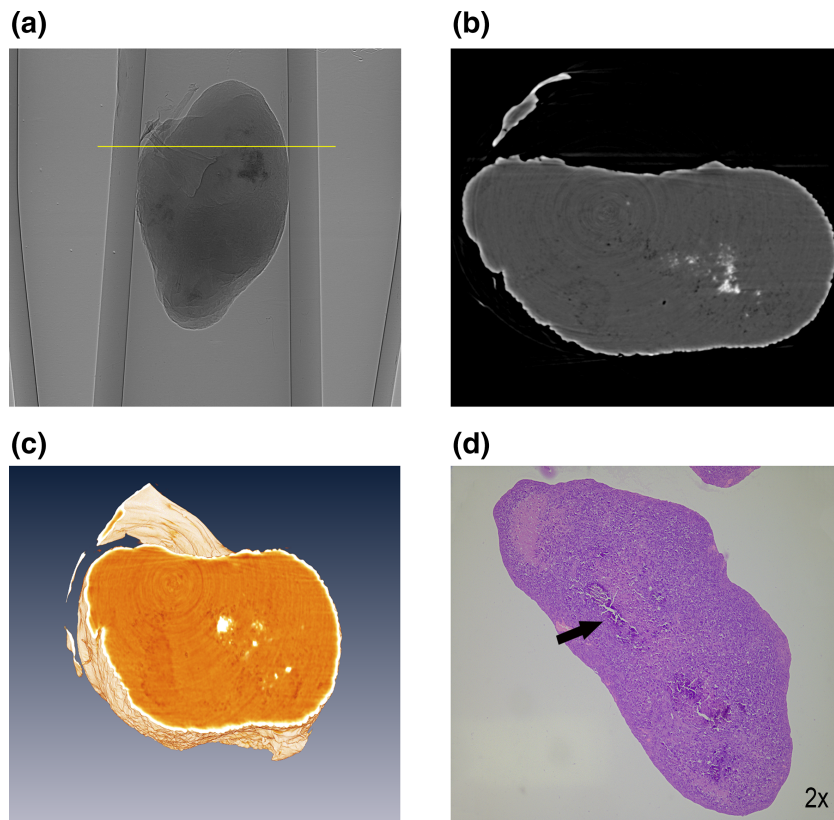
FIGURE 7: ILXPCI and pathologic image of nude mouse peritoneal metastasis in the control group at 14 days. a: An ILXPCI projective image of the specimen; horizontal line shows the slice we chose. b: The slice reconstruction image; white area shows the strong absorption. c: 3D-reconstruction image. d: Histopathological image; it shows the calcium deposition (black arrow).

was observed with X-ray in-line phase contrast imaging. ILXPCI presents a micron-scale imaging method that has potential applications in the treatment evaluation of peritoneal metastasis.

Our study has several limitations. First, because of the heterogeneous distribution of tumor tissue, the hand-drawn ROI on one axial MR image of the tumor used in our study may bring about sampling bias and may be less representative than the 3D measurement of the tumors. Second, the DKI parameter features of our animal model of gastric cancer were somewhat different from those of human patients. The b-factor selection in this research may not be optimal for the DKI model in patients, and further studies are needed to create a balance between the results from animal studies and the clinical practice requirement. Third, during the scanning process, we used clinical human wrist joint coils instead of using the animal coil, and the image quality improved, but the process was also cumbersome. Thus, more optimized imaging methods still need further discussion. Finally, the small animal sample sizes might result in bias in the results, and further investigation, with a larger number of animals, is needed to confirm the findings and to clarify the limitations of this study.

In conclusion, the present study suggests that DKI has the potential to detect therapy responses prior to morphological changes. The DKI parameters show a good correlation between the tumor tissue microstructure evaluation and the pathological results. The ADC and D values obtained by DKI are sensitive to detect tumor changes in the early stages, while the K parameter might be used as a noninvasive imaging biomarker for the whole process of the pathological changes in gastric cancer induced by TGF-β1 inhibition treatment. Our results also indicate that ILXPCI provides a potential preclinical mode of treatment evaluation in peritoneal metastasis.

Conflict of Interest

The authors have no conflicts of interest to declare.

Acknowledgment

References

1. Carcas LP. Gastric cancer review. J Carcinog 2014;13:14.

2. Ferro A, Peleteiro B, Malvezzi M, et al. Worldwide trends in gastric cancer mortality (1980-2011), with predictions to 2015, and incidence by subtype. Eur J Cancer 2014;50:1330–1344.

3. Ma F, Li W, Liu C, et al. MiR-23a promotes TGF-beta1-induced EMT and tumor metastasis in breast cancer cells by directly targeting CDH1 and activating Wnt/beta-catenin signaling. Oncotarget 2017;8:69538–69550.

4. Ebbing EA, Steins A, Fessler E, et al. Esophageal adenocarcinoma cells and xenograft tumors exposed to Erb-b2 receptor tyrosine kinase 2 and 3 inhibitors activate transforming growth factor beta signaling, which induces epithelial to mesenchymal transition. Gastroenterology 2017;153:63–76.e14.

5. Qu Y, Ray PS, Li J, et al. High levels of secreted frizzled-related protein 1 correlate with poor prognosis and promote tumourigenesis in gastric cancer. Eur J Cancer 2013;49:3718–3728.

6. Lin H, Yang G, Ding B, et al. Secreted frizzled-related protein 1 overexpression in gastric cancer: Relationship with radiological findings of dual-energy spectral CT and PET-CT. Sci Rep 2017;7:42020.

7. Therasse P, Arbuck SG, Eisenhauer EA, et al. New guidelines to evaluate the response to treatment in solid tumors. European Organization for Research and Treatment of Cancer, National Cancer Institute of the United States, National Cancer Institute of Canada. J Natl Cancer Inst 2000;92:205–216.

8. Ma H, Wei Y, Leng Y, et al. TGF-beta1-induced expression of Id-1 is associated with tumor progression in gastric cancer. Med Oncol 2014;31:19.

9. Hallinan JT, Venkatesh SK. Gastric carcinoma: imaging diagnosis, staging and assessment of treatment response. Cancer Res 2013;13:212–227.

10. Gaustad JV, Pozdniakova V, Hompland T, Simonsen TG, Rofstad EK. Magnetic resonance imaging identifies early effects of sunitinib treatment in human melanoma xenografts. J Exp Clin Cancer Res 2013;32:93.

11. Bozgeyik Z, Onur MR, Poyraz AK. The role of diffusion weighted magnetic resonance imaging in oncologic settings. Quant Imaging Med Surg 2013;3:269–278.

12. Martinez Barbero JP, Rodriquez Jimenez I, Martin Noguerol T, Luna Alcala A. Utility of MRI diffusion techniques in the evaluation of tumors of the head and neck. Cancers 2013;5:875–889.

13. Jensen JH, Helpern JA, Ramani A, Lu H, Kaczynski K. Diffusional kurtosis imaging: the quantification of non-Gaussian water diffusion by means of magnetic resonance imaging. Magn Reson Med 2005;53:1432–1440.

14. Van Cauter S, Veraart J, Sijbers J, et al. Gliomas: diffusion kurtosis MR imaging in grading. Radiology 2012;263:492–501.

15. Rosenkrantz AB, Sigmund EE, Johnson G, et al. Prostate cancer: feasibility and preliminary experience of a diffusional kurtosis model for detection and assessment of aggressiveness of peripheral zone cancer. Radiology 2012;264:126–135.

16. Nogueira L, Brandao S, Matos E, et al. Application of the diffusion kurtosis model for the study of breast lesions. Eur Radiol 2014;24:1197–1203.

17. Sun K, Chen X, Chai W, et al. Breast cancer: Diffusion kurtosis MR imaging—diagnostic accuracy and correlation with clinical-pathologic factors. Radiology 2015;277:46–55.

18. Chen Y, Ren W, Zheng D, et al. Diffusion kurtosis imaging predicts neoadjuvant chemotherapy responses within 4 days in advanced nasopharyngeal carcinoma patients. J Magn Reson Imaging 2015;42:1354–1361.

19. Almajdub M, Nejjari M, Poncet G, et al. In-vivo high-resolution X-ray microtomography for liver and spleen tumor assessment in mice. Contrast Media Mol Imaging 2007;2:88–93.

20. Snigirev A, Snigireva I, Kohn V, Kuznetsov S, Igor S. On the possibilities of X-ray phase contrast microimaging by coherent high-energy synchrotron radiation. Rev Sci Instrum 1995;66:5486–5492.

21. Wilkins SW, Gureyev T, Gao D, Pogany A, Stevenson A. Phase-contrast imaging using polychromatic hard x-rays. Nature 1996;384:335–338.

22. Fujima N, Yoshida D, Sakashita T, et al. Prediction of the treatment outcome using intravoxel incoherent motion and diffusional kurtosis imaging in nasal or sinonasal squamous cell carcinoma patients. Eur Radiol 2017;27:956–965.

23. Pang Y, Turkbey B, Bernardo M, et al. Intravoxel incoherent motion MR imaging for prostate cancer: an evaluation of perfusion fraction and diffusion coefficient derived from different b-value combinations. Magn Reson Med 2013;69:553–562.

24. Arponen O, Sudah M, Masarwah A, et al. Diffusion-weighted imaging in 3.0 Tesla breast MRI: Diagnostic performance and tumor characterization using small subregions vs. whole tumor regions of interest. PLoS One 2015;10:e0138702.

25. Wu H, Hu M, Liu Z, et al. Intravoxel incoherent motion diffusion-weighted MRI for characterizing regional variability and monitoring serial changes of parameters in rabbit VX2 liver tumors. J Magn Reson Imaging 2016;43:173–180.

26. Xu XQ, Hu H, Su GY, Liu H, Shi HB, Wu FY. Diffusion weighted imaging for differentiating benign from malignant orbital tumors: diagnostic performance of the apparent diffusion coefficient based on region of interest selection method. Korean J Radiol 2016;17:650–656.

27. Eisenhauer EA, Therasse P, Bogaerts J, et al. New response evaluation criteria in solid tumours: revised RECIST guideline (version 1.1). Eur J Cancer 2009;45:228–247.

28. Joo I, Lee JM, Han JK, Choi BI. Intravoxel incoherent motion diffusion-weighted MR imaging for monitoring the therapeutic efficacy of the vascular disrupting agent CKD-516 in rabbit VX2 liver tumors. Radiology 2014;272:417–426.

29. Landis JR, Koch GG. The measurement of observer agreement for categorical data. Biometrics 1977;33:159–174.

30. Fujima N, Yoshida D, Sakashita T, et al. Intravoxel incoherent motion diffusion-weighted imaging in head and neck squamous cell carcinoma: assessment of perfusion-related parameters compared to dynamic contrast-enhanced MRI. Magn Reson Imaging 2014;32:1206–1213.

31. Herbertz S, Sawyer JS, Stauber AJ, et al. Clinical development of galunisertib (LY2157299 monohydrate), a small molecule inhibitor of transforming growth factor-beta signaling pathway. Drug Des Devel Ther 2015;9:4479–4499.

32. Wang P, Wang YC, Chen XY, et al. CTHRC1 is upregulated by promoter demethylation and transforming growth factor-beta1 and may be associated with metastasis in human gastric cancer. Cancer Sci 2012;103:1327–1333.

33. Soldatos T, Ahlawat S, Montgomery E, Chalian M, Jacobs MA, Fayad LM. Multiparametric assessment of treatment response in high-grade soft-tissue sarcomas with anatomic and functional MR imaging sequences. Radiology 2016;278:831–840.

34. King AD, Chow KK, Yu KH, et al. Head and neck squamous cell carcinoma: diagnostic performance of diffusion-weighted MR imaging for the prediction of treatment response. Radiology 2013;266:531–538.

35. Kyriazi S, Collins DJ, Messiou C, et al. Metastatic ovarian and primary peritoneal cancer: assessing chemotherapy response with diffusion-weighted MR imaging—value of histogram analysis of apparent diffusion coefficients. Radiology 2011;261:182–192.

36. Yuan J, Yeung DK, Mok GS, et al. Non-Gaussian analysis of diffusion weighted imaging in head and neck at 3T: a pilot study in patients with nasopharyngeal carcinoma. PLoS One 2014;9:e87024.

37. Bains LJ, Zweifel M, Thoeny HC. Therapy response with diffusion MRI: an update. Cancer Imaging 2012;12:395–402.

38. Cui Y, Zhang XP, Sun YS, Tang L, Shen L. Apparent diffusion coefficient: potential imaging biomarker for prediction and early detection of response to chemotherapy in hepatic metastases. Radiology 2008;248:894–900.

39. Goyer P, Benoist S, Julie C, Hajjam ME, Penna C, Nordlinger B. Complete calcification of colorectal liver metastases on imaging after chemotherapy does not indicate sterilization of disease. J Visc Surg 2012;149:e271–274.

40. Khandakar B, Kumar L, Kumar S, et al. Tumour morphology after neoadjuvant chemotherapy as a predictor of survival in serous ovarian cancer: an experience from a tertiary care centre in India. Malays J Pathol 2015;37:115–121.